scientific reports

Check for updates

OPEN

# DFT investigation of efficient hydrogen storage utilizing Li and Na decorated co-doped graphene (B/N)

N. N. Mostafa[1,3], Kamal A. Soliman[2,3]✉, S. M. Abd El Haleem[1] & W. S. Abdel Halim[1]✉

**This study investigates the hydrogen storage capacity of co-doped graphene with non-bonded B and N atoms ($BC_4N$) using density functional theory (DFT). The optimized structure reveals the introduction of co-doping ripples the surface, enhancing potential hydrogen storage applications. The adsorption behavior of Li and Na atoms on the $BC_4N$ surface is examined, demonstrating a higher binding energy, surpassing their cohesive energies. Density of State (DOS), Partial Density of State (PDOS), and charge transfer analyses indicate electron donation from Li and Na to $BC_4N$ monolayer, establishing $BC_4N$ as an electron acceptor. The investigation extends to $H_2$ adsorption on Li/$BC_4N$ and Na/$BC_4N$ systems, revealing a non-dissociative form and a cooperative effect with increasing $H_2$ molecules. The hydrogen storage gravimetric density is calculated, and desorption temperatures are determined, highlighting the potential of Li/$BC_4N$ and Na/$BC_4N$ as promising candidates for efficient hydrogen storage.**

**Keywords** Hydrogen storage, Co-doped graphene, Li and na decoration, DOS, PDOS, Gravimetric density, Desorption temperature

The focus on hydrogen as an ideal energy resource has grown due to its favorable characteristics, including high energy density, renewability, and friendly to the environment. Its potential to replace fossil fuels has led to a significant emphasis on developing a stable and cost-effective storage system[1–6]. The US Department of Energy has a target for hydrogen storage capacity of 5.5 wt% of weight density[7], emphasizing the importance of achieving optimal binding energy for effective hydrogen recycling at near-ambient conditions[8,9]. Various carbon nanostructures, such as carbon nanotubes, and graphene have been investigated for their hydrogen adsorption capabilities, driven by their reversibility, fast kinetics, and high capacities[10–15]. The interest in the processes of adsorption and desorption with carbon-based materials from the intrinsic advantageous properties these materials possess. These include low density, high chemical stability, and the capacity to manipulate pore structures and surface areas, rendering them compelling options for hydrogen storage technologies[16]. Among carbon-based materials, the focus of research has notably turned towards graphene-based carbon materials. This shift is primarily driven by the extraordinary features exhibited by graphene, such as an exceptionally high specific surface area, mechanical flexibility, robustness, and a lightweight composition. These attributes position graphene as a promising candidate for hydrogen storage devices, emphasizing its potential for practical applications[17].

Furthermore, graphene an exceptional two-dimensional carbon material known for its distinctive properties has become a focal point of research interest due to recent advancements in its large-scale production[18]. Apart from its prevalent applications in electronics, graphene plays a pivotal role in sensor production and serves as a molecular adsorbent. While previous studies extensively explored graphene's efficacy in adsorbing various small molecules, its potential as hydrogen ($H_2$) adsorbent is limited, and hydrogen passivation may even compromise the mechanical properties of graphene[19]. To address these challenges, sophisticated techniques are necessary for effective hydrogen uptake. Some studies have opted for innovative approaches, such as utilizing curved graphene or graphene hollows to enhance interactions with $H_2$/adsorbent[20]. On the other hand, alternative strategies involve employing planar graphene sheets with doped heteroatoms. Transition metals such as titanium (Ti)[21], iron (Fe)[22], nickle (Ni)[23], palladium (Pd)[24], and platinum (Pt)[25] can be useful for this purpose.

[1]Department of Chemistry, Faculty of Science, Zagazig University, P.O.Box 44519, Zagazig, Egypt. [2]Department of Chemistry, Faculty of Science, Benha University, P.O. Box 13518, Benha, Egypt. [3] N. N. Mostafa, Kamal A. Soliman contributed equally to this work as first authors. ✉email: kamalsoliman@gmail.com; kamal.soliman@fsc.bu.edu.eg; wsahalim@zu.edu.eg

Ao et al. explored Al-doped porous graphene by DFT study. Their investigations demonstrated the efficient adsorption of $H_2$ molecules by such structures with adsorption energy of −0.41 eV[15]. Huo et al. employed theoretical methods to investigate Ti-decorated boron-doped porous graphene in adsorbing $H_2$ molecules[26]. They investigated that boron-doped porous graphene decorated with titanium atoms can consistently capture sixteen hydrogen molecules, achieving a gravimetric hydrogen uptake of 8.58 wt%.

Researchers conducted both experimental and theoretical investigations on graphene to enhance hydrogen storage capacity. The studies revealed that modifying the electronic properties of dispersed carbon-based materials through doping with nonmetallic elements (such as B and N) or intentionally creating vacancies could be a promising strategy. This approach has been shown to enhance the adsorption performance of hydrogen according to various works[27,28]. Yang et al.[29] demonstrated that, under conditions of 298 K and 10 Mpa, the hydrogen storage capacity increased to 1.2 wt% through hydrogen spillover on ruthenium-decorated boron-doped microporous carbon. In the study conducted by Wu and colleagues[30], they observed that B-doped graphene has a superior ability to adsorb hydrogen compared to pristine graphene. This increased adsorption capability is attributed to the presence of low activation barriers, particularly under ambient conditions. Furthermore, Lee et al.[31] conducted research on the utilization of Li-decorated graphene for hydrogen storage. In this study, they introduced nitrogen defects that are experimentally feasible to enhance the overall performance of the hydrogen storage system.

This study introduces an approach by suggesting a unique arrangement of graphene sheets that co-doped with boron and nitrogen and featuring Li, and Na atoms to enhance hydrogen storage. The B, and N atoms co-doped graphene are non-bonded that be more efficient catalyst when compared to bonded B-N co-doped graphene[32,33].To assess the influence of this co-doped structure on hydrogen adsorption, the study utilizes first-principle analyses based on density functional theory (DFT).

## Results and discussion

### Structural properties of co-doped graphene (B and N atom), decorated by li, and Na atom

To explore the hydrogen storage capacity of co-doped graphene with B, and N atom that is non-bonded, the optimized geometry of this system ($BC_4N$) is shown in Fig. 1, and the corresponding data are compiled in Table 1. A vibrational frequency calculation was also performed on the optimized BC4N sheet (B3LYP/6-31G(d, p)); no imaginary frequencies were found, confirming that the structure shown in Fig. 1 corresponds to a true local minimum. As seen in Table 1, the bond lengths between B-C, C-C, and C-N are 1.50 Å, 1.43 Å, and 1.41 Å respectively. The structure of pristine graphene is flat and by co-doped with B, and N atom that are non-bonded, the presence of ripples appears that is may be effective in hydrogen storage application. Initially, the study of binding of single atom decorated the surface such as Li, and Na atoms was determined. As seen in Fig. 2, the optimized Li, and Na atom on the $BC_4N$ surface are prefer to be adsorbed on hollow center of the hexagon and Cartesian coordinates for the Li/$BC_4N$ and Na/$BC_4N$ are shown in Table S1 and S2. This corresponds well with the preferred site for Li atom adsorption on both pure graphene and porous graphene[2,34,35]. In the optimized structures, the distance between Li/Na and nearest carbon atom is 2.17/2.53 Å, respectively as presented in Table 1. The binding energies for Li and Na atom over the surface were found to be −2.51 eV, and − 1.95 eV respectively that is higher than their cohesive energies[36,37]. The results show that co-doped graphene with B, and N atom has the capacity to significantly enhance the binding energy of Li, and Na atoms, exceeding the cohesive energy of Li and Na. This intentional effect results in the suppression of Li, and Na adatom clustering on $BC_4N$ system. Therefore, co-doped graphene with B, and N atom demonstrates significant potential for hydrogen storage due to its characteristic of maintaining geometric stability.

The interaction of the adsorbed Li, and Na atom on the $BC_4N$ system were also studied by calculating the Density of State (DOS), Partial Density of State (PDOS), and charge transfer that obtained from natural bond orbital (NBO). The analysis reveals an electronic charge transfer from the Li, and Na adatom to the substrate, as illustrated in Table 1. Essentially, the adsorbent functions as an electron acceptor in relation to the Li, and Na adatom. Based on these results, it can be inferred that $BC_4N$ systems exhibit a higher binding energy for Li, and Na adatoms on the surface. Despite the fact that the charge transfer from Na to $BC_4N$ surface is greater than that from Li, the binding energy of Li on BC4N is greater. This seemingly strange finding can be explained by the fact that both Li and Na are electrostatically attracted to $BC_4N$ π-electrons. Li atom experiences stronger electrostatic attraction than Na atom due to its smaller size and higher nuclear charge, and the smaller size of Li allows its orbitals to overlap more efficiently with BC4N π-orbitals, developing stronger covalent bonding, whereas Na atom's larger size makes its orbital overlap with BC4N less optimal, limiting the covalent contribution to its binding. By analyzing the density of states (DOS) and projected density of states (PDOS) as seen in Fig. 3, The observation that peaks in the density of states (DOS) increase after decorating BC4N with Li, and Na atom. When Li and Na atom are deposited on BC4N surface, they interact with its π-electron system and this interaction can be understand by PDOS. The Fig. 3, when Li atom sit on hollow site, its 2s-orbital of Li atom directly overlap with the 2p orbitals of the surrounding C, B, and N atom in the BC4N surface at energies − 1.64 eV, 1.39 eV, and 3.25 eV. Also, Na decorated BC4N surface show overlap between 3s-orbital of Na atom with 2p orbitals of the C, B, nad N atom in the BC4N surface at energies 0.55 eV, at −2.24 eV and 1.99 eV there is overlap between 3s-orbital of Na atom with 2p-orbitals of N and C atom of the BC4N surface.

### Hydrogen storage properties

The optimized structures of $H_2$ adsorbed on Li/$BC_4N$ and Na/$BC_4N$ systems are illustrated as seen Figs. 4 and 5. The Cartesian coordinates for $H_2$ adsorbed on the Li/$BC_4N$ and Na/$BC_4N$ are shown in Table S1 and S2. The PDOS of $H_2$ molecules on Li/$BC_4N$ and Na/$BC_4N$ are seen in Figs 6 and 7. During the optimization of the first molecule of $H_2$ on Li/$BC_4N$ and Na/$BC_4N$ systems, the $H_2$ adsorbed on Li, and Na with tilted orientation on a lithium and sodium atom and This initial configuration establishes a specific binding geometry. By analyzing the

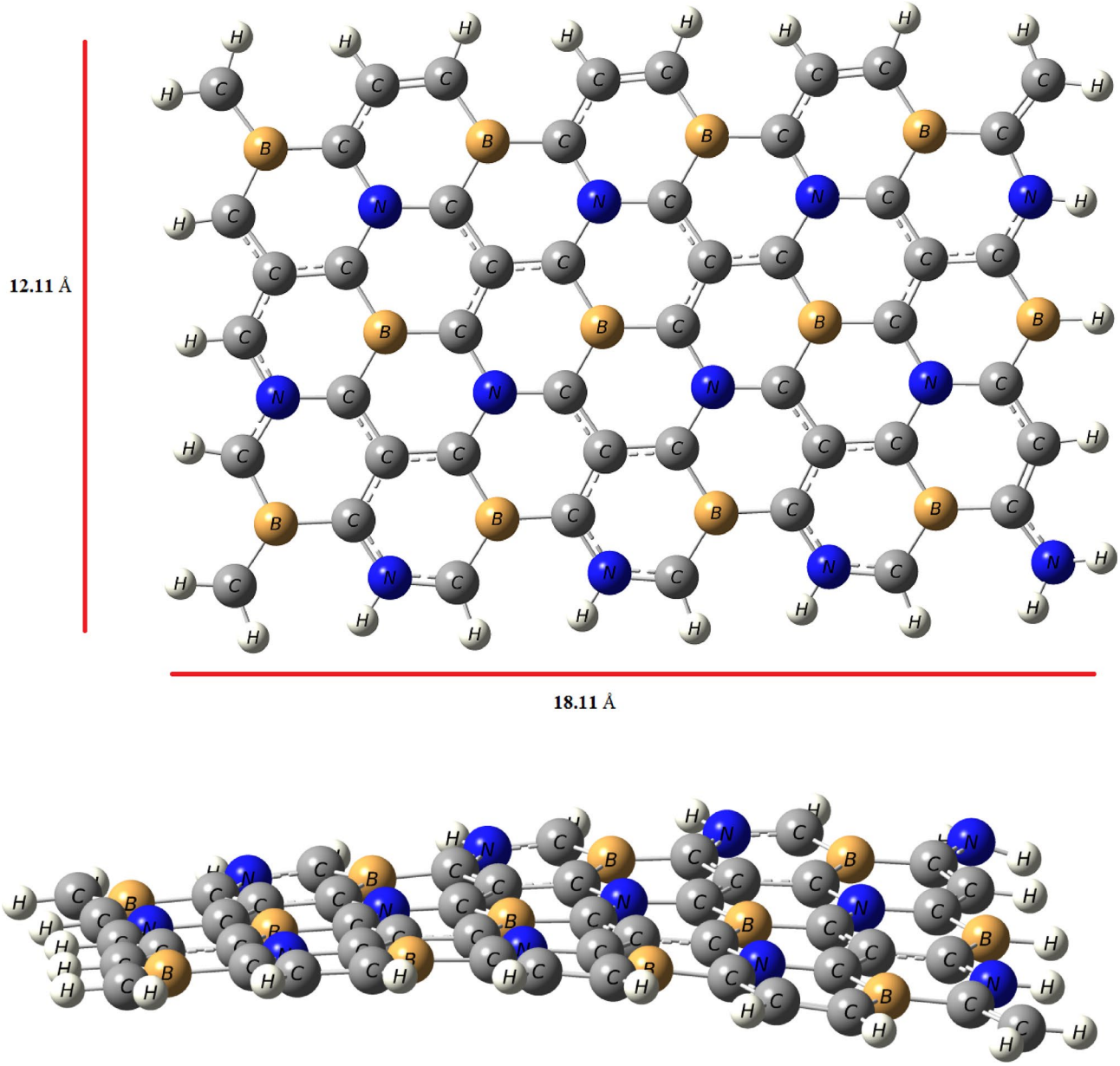


**Fig. 1**. The optimized structure of B, and N co-doped graphene; top- (up) and side- (down) view.

| System | d (Å) | $E_b$(eV) | $Q_{NBO}$(e) |
|---|---|---|---|
| $BC_4N$ | 1.50 (B-C)<br>1.43 (C-C)<br>1.41 (N-C) | | |
| $Li/BC_4N$ | 2.17 (Li-C) | −2.51 | 0.90 (Li) |
| $Na/BC_4N$ | 2.53 (Na-C) | −1.95 | 0.95 (Na) |

**Table 1**. Equilibrium distance (d, Å), binding energies of li, and Na decorated BC4N monolayer and the charge.

results that collected in Tables 2 and 3, we can find out that the adsorption energy of −0.12 eV, and, the distance of $d_{Li-H}$ is 2.09 Å in $H_2/Li/BC_4N$, and the distance of $d_{Na-H}$ is 2.49 Å in $H_2/Na/BC_4N$. For each configuration the H-H bond lengths of $H_2$ molecules are 0.75 Å, which are consistent with the calculated free $H_2$ molecule (0.750 Å), indicating that the adsorbed $H_2$ molecule is in the non-dissociative form. To further validate the physisorptive nature and reliability of our $H_2$ adsorption data, we re-examined the H-H bond length before and after adsorption. In our calculations (GGA-PBE + D3), the free $H_2$ bond length is 0.750 Å, and upon adsorption

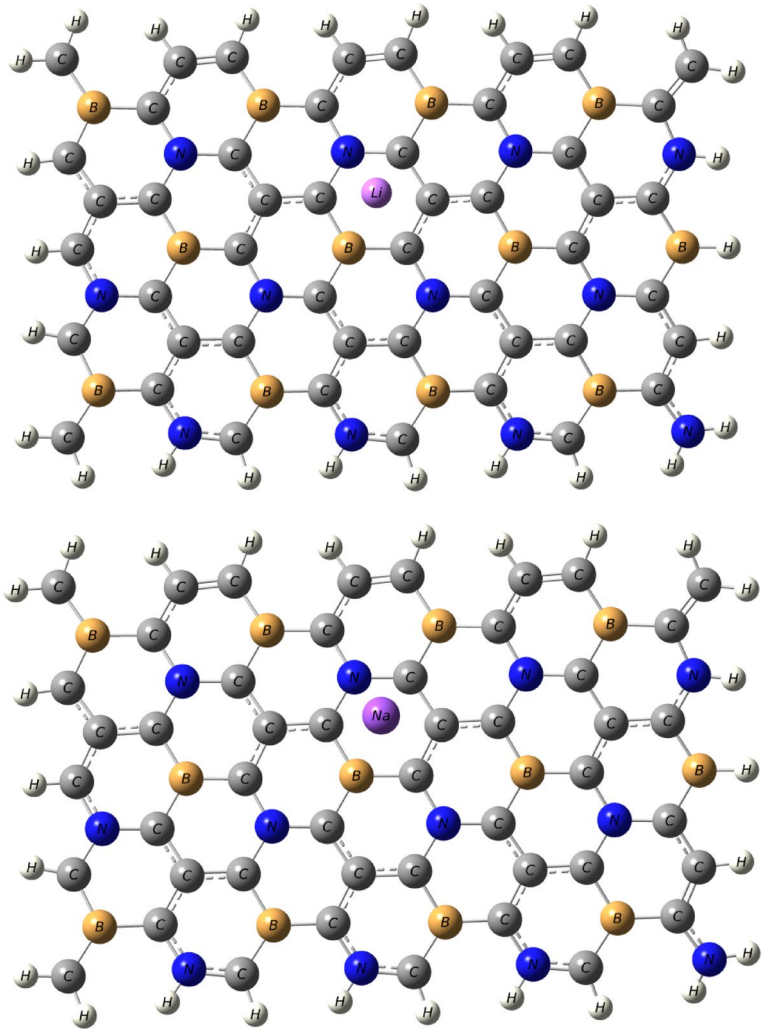


**Fig. 2**. The optimized structure of Li "up", and Na "lower" decorated $BC_4N$ monolayer.

it remains 0.750 Å. This negligible change is fully consistent with the findings of Dange et al.[38], who report that charge polarization driven $H_2$ physisorption on $NLi_4$ decorated boron phosphide biphenylene induces an H-H elongation of only ≈ 0.003 Å. Therefore, the unchanged H-H distance in our system confirms that we are describing a true physisorption process with no spurious chemisorption artifacts. The adsorption of another hydrogen molecule on the opposite side of the Li and Na decorated $BC_4N$ system. The adsorption energy increases to −0.27 eV for Li/$BC_4N$ and −0.19 eV for Na/$BC_4N$ surface, suggesting a stronger interaction. The charge on Li is 0.85e, on Na is 0.93e and the charges of $H_2$ on Li and Na are 0e,0.04e, 0.04e,−0.03e respectively. This indicates potential charge redistribution within the system, impacting bonding and stability. The high dipole moment (19.86 Debye and 19.60 Debye) for the first adsorbed $H_2$ molecule signifies significant polarization, implying the $H_2$ molecule is distorted upon interaction with the Li and Na atom. The rippling of the $BC_4N$ surface evident in Figs. 4 and 5 arises directly from the physisorption of $H_2$, the weak van der Waals interaction and slight charge polarization at the adsorption site pull the nearest B and N atoms out of the plane, producing the observed distortion. To ensure that these distorted geometries are true minima, we have performed full vibrational frequency calculations on each $H_2$ adsorbed configuration with no imaginary modes, confirming that the rippled structures are stable adsorption complexes rather than transition state artifacts .

With an increasing number of hydrogen molecules, a noteworthy trend is observed. The adsorption energy continues to increase that the two, Three, and four $H_2$ molecules on Li/$BC_4N$ surface are −0.19 eV, −0.25 eV, and −0.27 eV respectively. Binding strength increases with the number of adsorbed $H_2$ molecules, reaching a maximum with four molecules (−0.27 eV). This suggests cooperative effects enhance binding as more $H_2$ are present. As shown in Table 2, the distance between Li decorated $BC_4N$ surface are 2.17Å, 2.18 Å for the two $H_2$ molecules, 2.24Å, 2.30Å, 2.26Å for the three $H_2$ molecules on Li/BC4N surface, but when the four $H_2$ molecules we found that one $H_2$ is far away from the Li decorated $BC_4N$ surface, and the charges obtained from NBO of Li atom is decreased by increasing $H_2$ molecules adsorbed as seen in Table 2 implying a cumulative effect of hydrogen adsorption. Simultaneously, the charge on lithium decreases. This suggests a dynamic charge transfer during the adsorption process. Li-H distances and charge transfer to $H_2$ molecules slightly increase with more

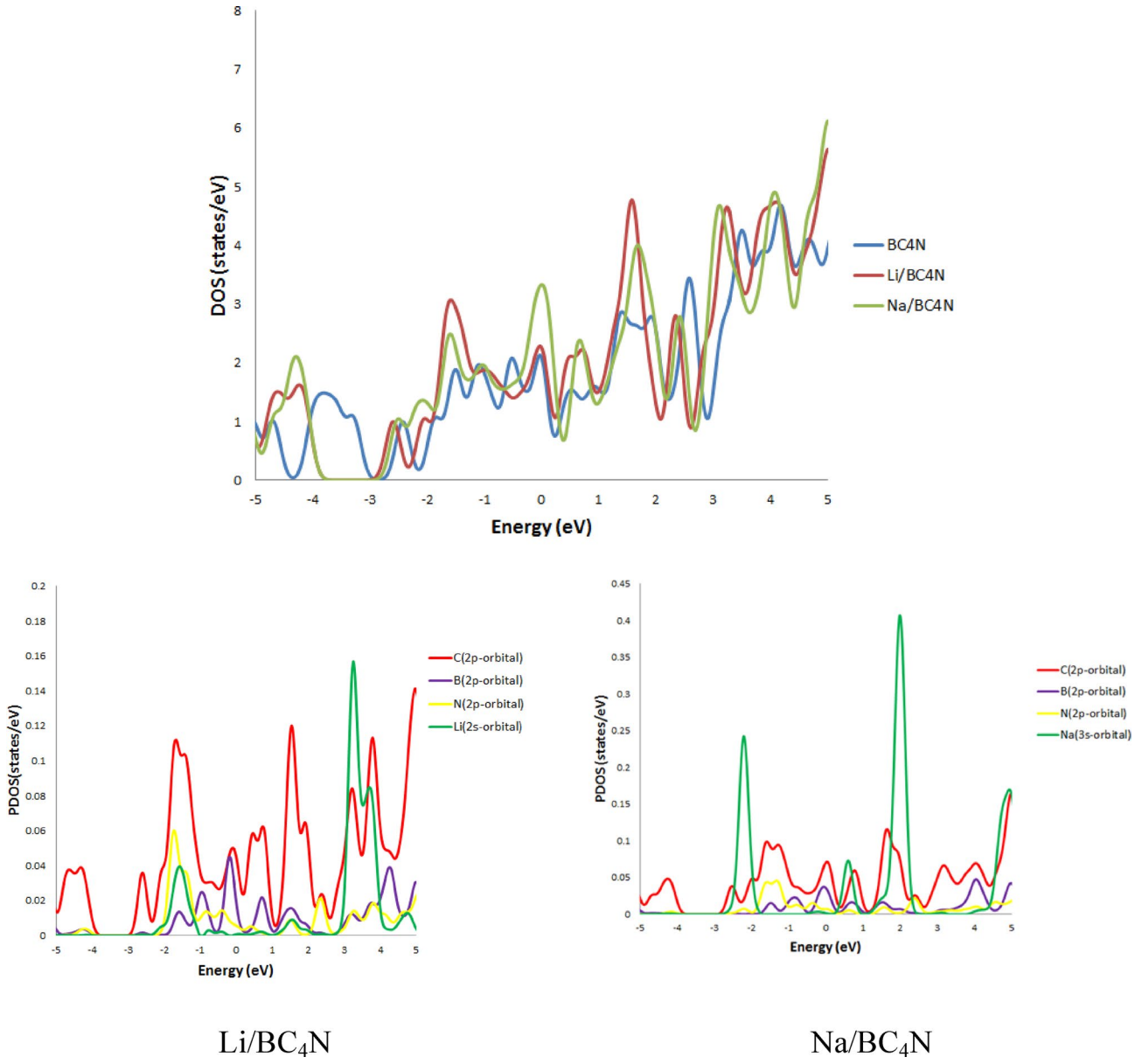


**Fig. 3**. Total DOS and PDOS of $BC_4N$ and Li, Na atom decorated $BC_4N$ surfaces.

$H_2$ adsorption. This indicates stronger electrostatic interactions between Li and $H_2$ molecules. As shown in Fig. 8, regions of electron accumulation (yellow) appear primarily around the Li and Na sites and the nearest $H_2$ molecules, while corresponding depletion (cyan) is observed on adjacent B and N atoms. This polarization pattern confirms that $H_2$ adsorption is driven by charge–induced dipole interactions at the metal centers, reinforcing the physisorptive mechanism without covalent bond formation. The increasing adsorption energy with multiple $H_2$ molecules and efficient utilization of Li sites are encouraging characteristics. As seen in Table 3, we observed in $Na/BC_4N$ surface that the recorded adsorption energies of two, three, and four $H_2$ molecules are −0.19 eV, −0.25 eV, and −0.23 eV respectively. Also as seen in Table 3, the distance between Na-H are 2.52Å, 2.50Å for two $H_2$ molecules, 2.55Å, 2.56Å, 2.52Å, and one $H_2$ molecules are far away when adsorbing four $H_2$ molecules. The distances of H-H bond are in range 0.74Å–0.75Å. To account for dispersion interaction, DFT-D3 method, the adsorption energy of hydrogen molecules on Li and Na decorated $BC_4N$ surface as listed in Tables 2 and 3 are lower when using the Grimme D3 dispersion correction. D3 adds an attractive dispersion term to the potential energy surface, accounting for the weak interaction between hydrogen molecules with the Li and Na decorated $BC_4N$ surface. This stronger attractive interaction leads to a lower (more negative) adsorption energy, indicating a more stable binding.

As seen in Table 2 dipole moment of Li-decorated graphene increases with the number of adsorbed $H_2$ molecules (from 12.87 Debye for two $H_2$ to 13.57 Debye for four $H_2$) is an interesting phenomenon with potential implications for hydrogen storage and other applications. When $H_2$ interacts with Li or Na on BC4N surface, charge transfer occurs. $H_2$ slightly donates some electron density to the Li, and Na atom, creating a small

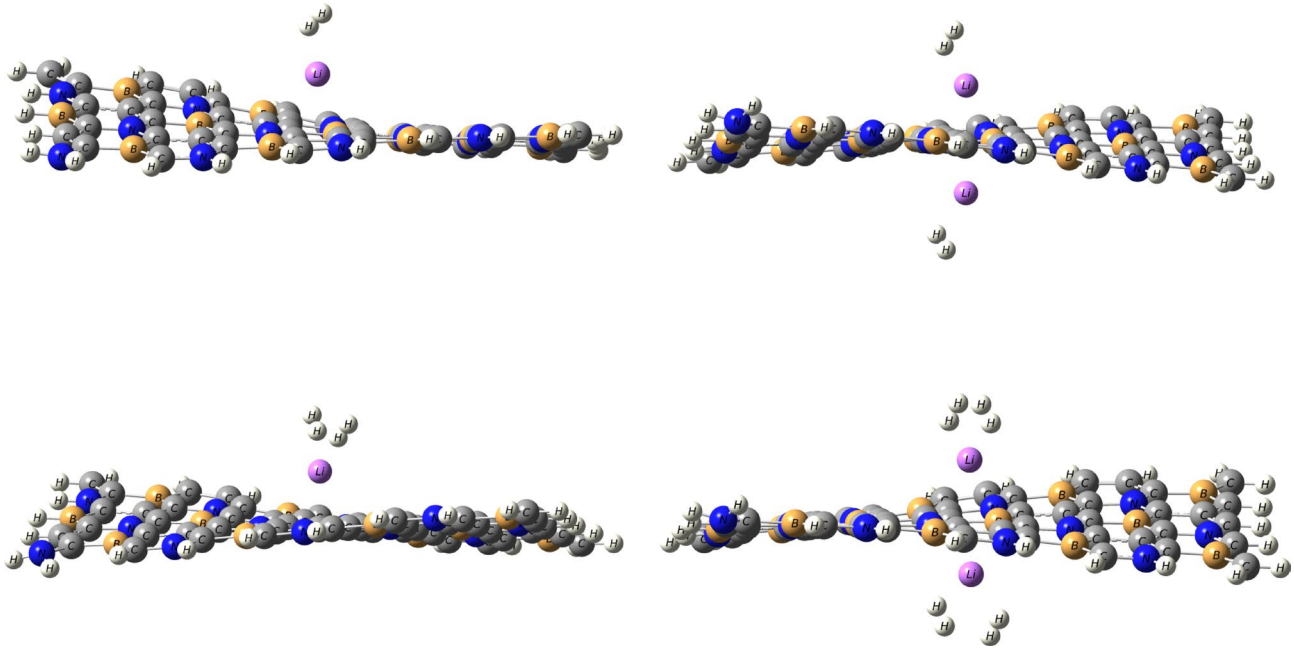

**Fig. 4**. Optimized structures of $H_2$ molecules on Li/$BC_4N$ monolayer.

individual dipole moment around each $H_2$-Li, and $H_2$-Na pair. When the $H_2$ adsorbs on the opposite side of Li or Na atom decorated $BC_4N$ surface, its individual dipole moment might partially cancel out the dipole moment created by the $H_2$ molecules that adsorbed on one side. This could occur if the two $H_2$ molecules are oriented in a specific way, with their positive and negative ends pointing towards each other.

The partial density of states (PDOS) provides valuable insights into the electronic interactions between adsorbed $H_2$ molecules and the Li- and Na- decorated $BC_4N$ surface, as shown in Figs. 6 and 7. The third hydrogen molecule's adsorption energy on Li, Na atom decorated $BC_4N$ surface is slightly higher than the initial two, as depicted in Tables 2 and 3. This behavior is elucidated by examining the Partial Density of States (PDOS). The energy bands associated with absorbed $H_2$ molecules exhibit splitting below the Fermi.

level when increasing hydrogen molecules at $\sim -14$ eV. This observation implies interplay between the absorbed hydrogen molecules, indicating a potential interaction between them and proposed to enhance the adsorption strength of the third hydrogen molecule, resulting in the elevated adsorption energy. Additionally, the overlap of $H_2$ orbitals with Li-2s in specific energy intervals from − 1 eV to 5 eV, and from − 2 eV to 4 eV for the overlap $H_2$−1s orbitals with Na-3s orbitals signifies electrostatic interactions.

In determining the maximum hydrogen storage gravimetric density (GD) of Li and Na decorated $BC_4N$ monolayers, a systematic addition of both metal atoms and $H_2$ molecules is required. For the Li and Na atom decorated $BC_4N$ monolayer, it was observed that three $H_2$ molecules on the upper layer represent the maximum capacity, as adding an extra $H_2$ molecule is too distant from the decorated atom. In the case of decorating both sides with Li and Na on the BC4N monolayer, the maximum storage capacity increased to six $H_2$ molecules. The gravimetric capacity is calculated by the following equation:

$$\mathrm{GD} = \frac{nm_{H2}}{m_{adsorbent+}\, nm_{H2}} \times 100\% \tag{1}$$

Where $nm_{H2}$, and $m_{adsorbent}$ are the mass of $H_2$ molecules and mass of adsorbent respectively. n is the number of hydrogen molecules. By using the above equation, Li/$BC_4N$ storage 12.2 % of hydrogen molecules, and Na/$BC_4N$ has 9.2 % storage capacities.

Desorption temperature represents the temperature at which hydrogen molecules, previously adsorbed onto a storage material, are released from the material, making the stored hydrogen available for use. The desorption temperature is a critical parameter in hydrogen storage systems, influencing the efficiency and practicality of the release process. Understanding and optimizing desorption temperatures is essential for designing.

effective storage materials. The hydrogen desorption temperature (TD) in a hydrogen storage system can be approximated using the Van't Hoff formula[39]:

$$T_D = -\frac{E_{ads}}{K_B}\left(\frac{\Delta S}{R} - ln\frac{p}{p^{\circ}}\right)^{-1} \tag{2}$$

Where $K_B$ is Boltzmann constant, $\Delta S$ is the entropy change from gas to liquid phase of H2 molecule, R is the universal gas constant, $p^{\circ}$ and p are standard atmospheric pressure (1 atm) and equilibrium pressure respectively[40–42]. The $T_D$ for $6H_2$\$2Li/$BC_4N$, and $6H_2$\$2Na/$BC_4N$ are 745 K and 664 K respectively. The

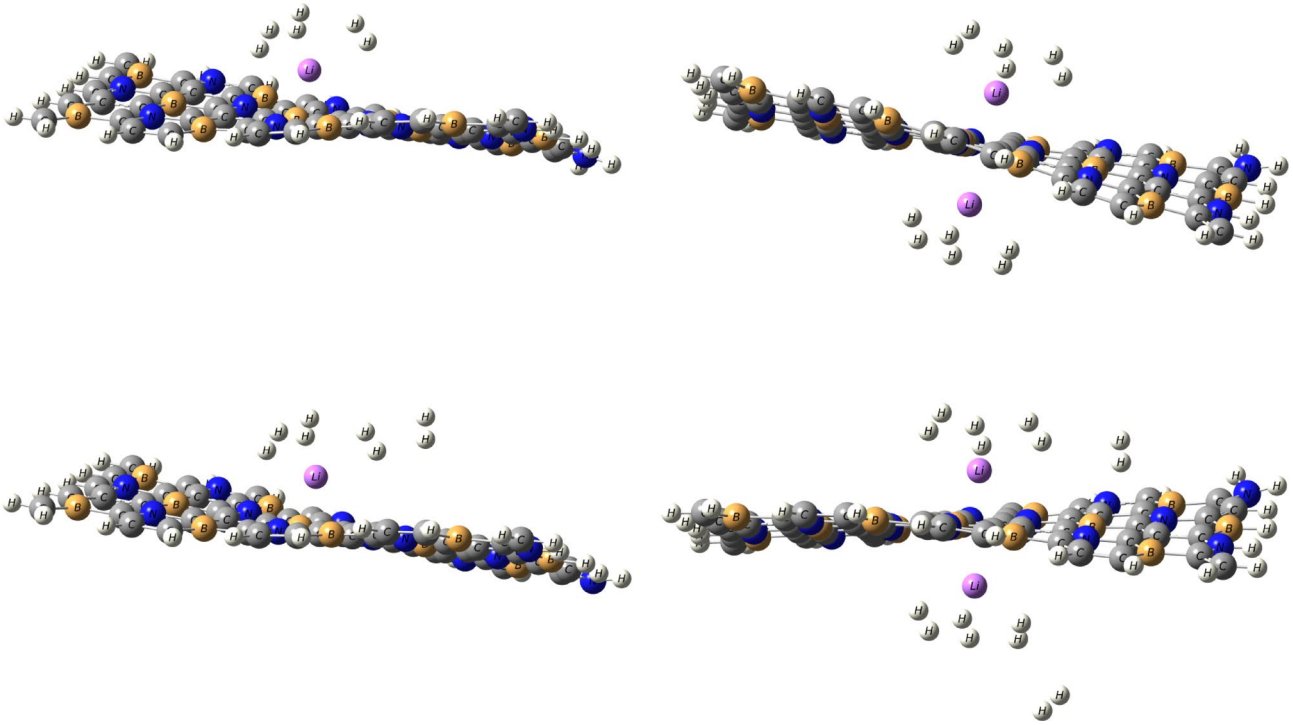

**Fig. 4.** (continued)

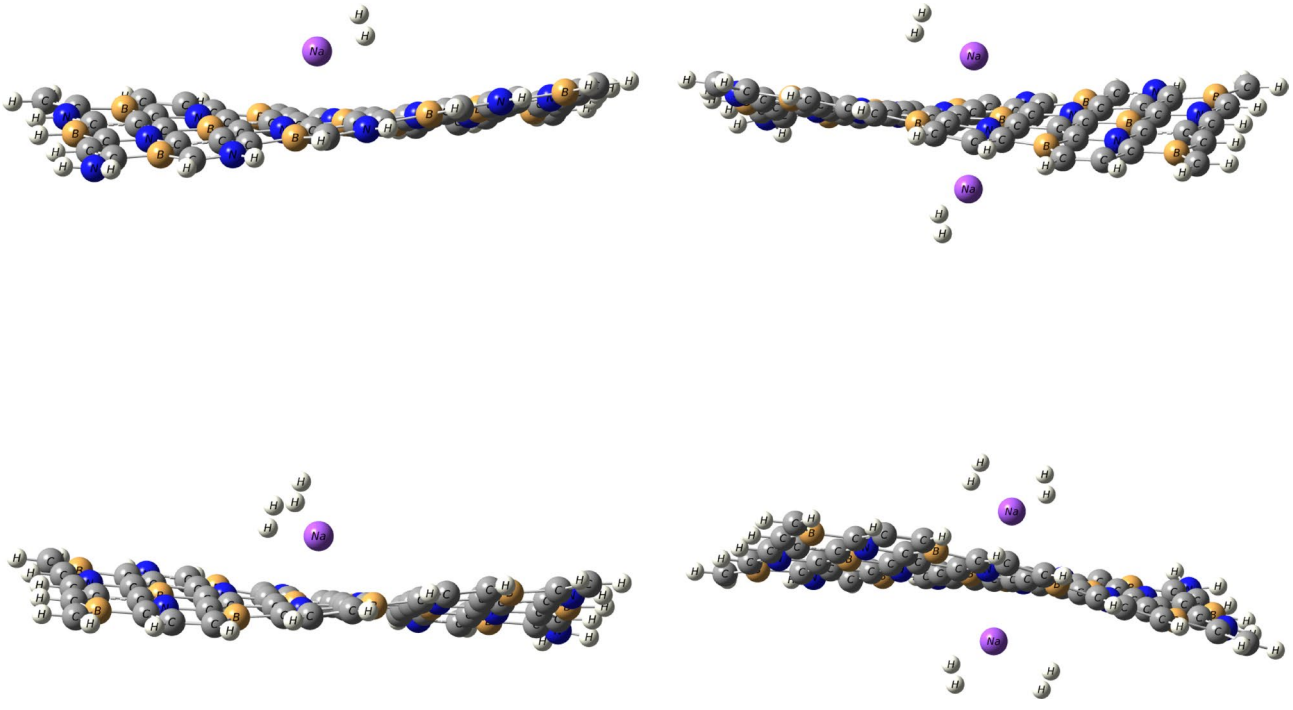

**Fig. 5**. Optimized structures of $H_2$ molecules on $Na/BC_4N$ monolayer.

connection between the desorption temperature of $H_2$ molecule and the applied pressure, noting that a decrease in pressure leads to a lower $T_D$. This trend is explained by the proportional association between the chemical potential of $H_2$ gas and pressure. Utilizing this insight, it becomes possible in practical scenarios to achieve the release of all stored $H_2$ molecules at temperatures considered acceptable by effectively modulating the pressure.

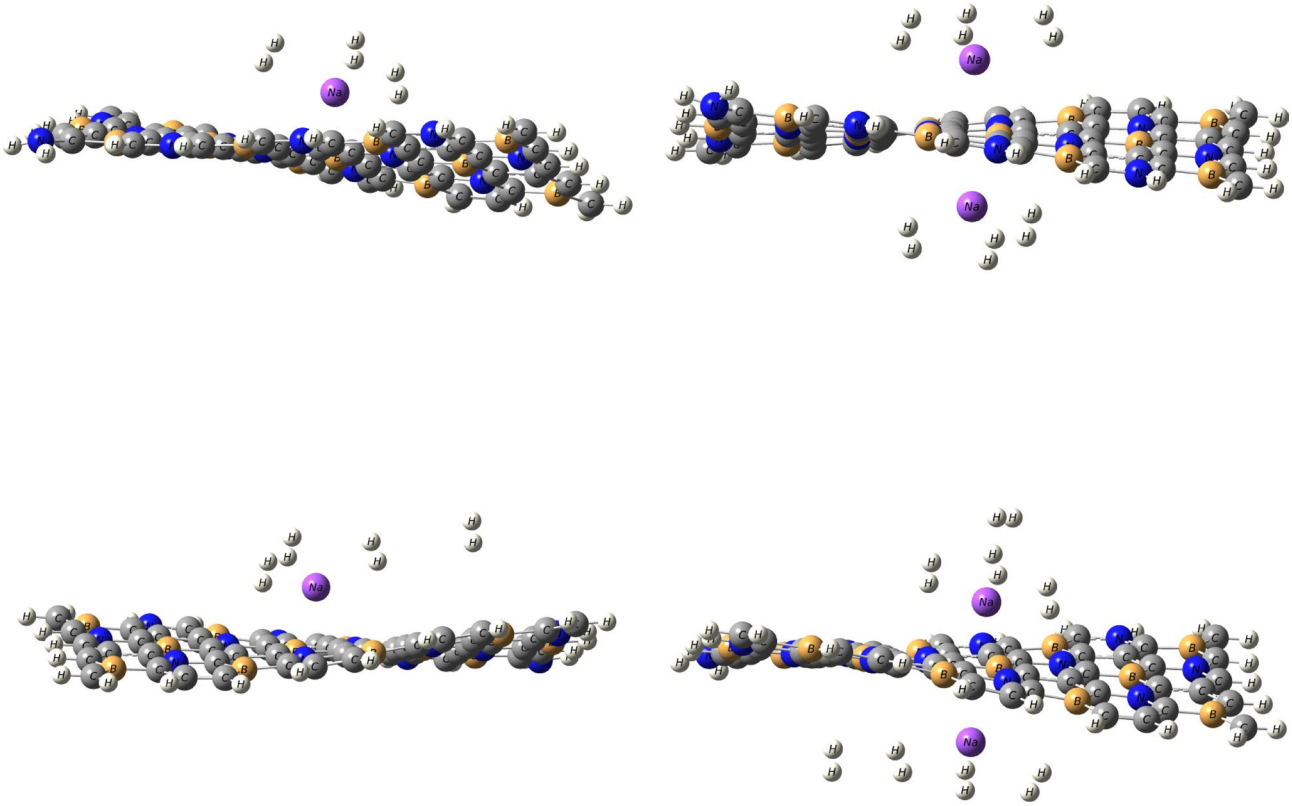

**Fig. 5.** (continued)

| System | $d_{Li-H}$(Å) | $d_{H-H}$(Å) | $E_{ads}$(eV) | $Q^{Li}$(e) | $Q^{H}$(e) | μ (Debye) |
|---|---|---|---|---|---|---|
| $1H_2$\$Li/$BC_4N$ | 2.09 | 0.75 | −0.12 (−0.21) | 0.82 | 0.03, 0.01 | 19.86 |
| $2H_2$\$Li/$BC_4N$ | 2.18, 2.17 | 0.75 | −0.19 (−0.36) | 0.74 | 0.02, 0.03, 0.04, 0.01 | 12.87 |
| $3H_2$\$Li/$BC_4N$ | 2.24, 2.30, 2.26 | 0.75 | −0.25 (−0.48) | 0.66 | 0.04, 0.01, 0.01, 0.04, 0.06, −0.00 | 12.91 |
| $4H_2$\$Li/$BC_4N$ | 6.04, 2.24, 2.31, 2.26 | 0.74, 0.75 | −0.27 (−0.59) | 0.66 | 0.04, 0.01, 0.01, 0.04, 0.06, −0.00, 0.01, −0.01 | 13.57 |
| $2H_2$\$$Li_2$/$BC_4N$ | 2.10, 2.10 | 0.75 | −0.27 | 0.85, 0.85 | 0.04, 0.00, 0.04, 0.00 | 8.00 |
| $4H_2$\$$Li_2$/$BC_4N$ | 2.18, 2.15, 2.18, 2.15 | 0.75 | −0.45 | 0.77, 0.77 | 0.01, 0.04, 0.05, 0.00, 0.01, 0.04, 0.04, 0.00 | 8.29 |
| $6H_2$\$$Li_2$/$BC_4N$ | 2.25, 2.24, 2.22, 2.23, 2.21, 2.28 | 0.75 | −0.59 | 0.68, 0.68 | 0.05, 0.00, 0.01, 0.04, 0.05, 0.01, 0.01, 0.04, 0.05, 0.01, 0.00, 0.05 | 8.12 |
| $8H_2$\$$Li_2$/$BC_4N$ | 6.53, 2.25, 2.24, 2.22, 4.60, 2.22, 2.20, 2.28 | 0.74, 0.75 | −0.61 | 0.68, 0.68 | 0.05, 0.00, 0.01, 0.04, 0.05, 0.01, 0.01, 0.04, 0.05, 0.01, 0.00, 0.05, 0.01, −0.00, 0.01, −0.02 | 8.28 |

**Table 2**. Structural and energetic properties for the hydrogen molecule adsorbed on Li/BC4N on one and two sided. The smaller Li-H distance ($d_{Li-H}$), the bond length of H-H, charge transfer (Q), dipole moment (μ).

## AIMD *computations*

To assess the thermal and structural stability of the $H_2$ adsorbed complexes at finite temperature, we performed ab initio molecular dynamics (AIMD) simulations (300 K, and Berendsen thermostat) on the $3H_2$\$Li/$BC_4N$ and $3H_2$\$Na/$BC_4N$ systems. Figure 9 shows that the temperature remains well controlled around 300 K, and Fig. 9 illustrates that the total energies of both systems fluctuate within a narrow window of ±0.02 eV, with no drift towards positive energies. Visual inspection of snapshots throughout the 10 ps trajectory revealed no bond breaking or surface reconstructions. These results confirm that the Li- and Na- decorated $BC_4N$ monolayers can stably host up to three $H_2$ molecules at ambient conditions, with both structural integrity and adsorption reversibility maintained.

| System | $d_{Na-H}$(Å) | $d_{H-H}$(Å) | $E_{ads}$(eV) | $Q^{Na}$(e) | $Q^{H}$(e) | μ (Debye) |
|---|---|---|---|---|---|---|
| $1H_2$\$Na/$BC_4N$ | 2.49 | 0.75 | −0.12 (−0.14) | 0.92 | 0.05,−0.03 | 19.60 |
| $2H_2$\$Na/$BC_4N$ | 2.52,2.50 | 0.75 | −0.19 (−0.33) | 0.87 | −0.01, 0.03, 0.05, −0.03 | 19.06 |
| $3H_2$\$Na/$BC_4N$ | 2.55,2.56,2.52 | 0.75 | −0.25 (−0.41) | 0.81 | 0.04,−0.01,0.00, 0.03,0.05,−0.02 | 12.90 |
| $4H_2$\$Na/$BC_4N$ | 2.53,2.53,2.52,6.18 | 0.74, 0.75 | −0.23 (−0.53) | 0.81 | 0.04,−0.01, 0.00, 0.03,0.05, −0.02, 0.01, −0.01 | 19.29 |
| $2H_2$\$$Na_2$/$BC_4N$ | 2.48,2.52 | 0.75 | −0.19 | 0.93, 0.93 | 0.04,−0.03, 0.04,−0.03 | 7.20 |
| $4H_2$\$$Na_2$/$BC_4N$ | 2.52,2.49,2.50,2.53 | 0.75 | −0.35 | 0.89, 0.89 | −0.01,0.03,0.04, −0.02, −0.01,0.03, 0.04,−0.02 | 7.41 |
| $6H_2$\$$Na_2$/$BC_4N$ | 2.54,2.54,2.54, 2.52,2.55,2.54 | 0.75 | −0.52 | 0.83, 0.83 | 0.04,−0.02,−0.01, 0.04,0.04,−0.02, −0.01,0.03,0.04, −0.02, −0.02, 0.05 | 7.25 |
| $8H_2$\$$Na_2$/$BC_4N$ | 2.54,2.54,2.54,6.39, 2.57,2.59,2.55,2.85 | 0.74, 0.75 | −0.56 | 0.83, 0.78 | 0.04,−0.02,−0.01, 0.04,0.04,−0.02, −0.01, 0.03,0.05, −0.02,−0.02,0.05, 0.01,0.01,0.02, −0.02 | 7.29 |

**Table 3**. Structural and energetic properties for the hydrogen molecule adsorbed on Na/$BC_4N$ on one and two sided. The smaller Na-H distance ($d_{Na-H}$), the bond length of H-H, charge transfer (Q), dipole moment (μ).

## Conclusion

Co-doped graphene ($BC_4N$) exhibits favorable characteristics for hydrogen storage applications. The co-doping introduces structural ripples, enhancing binding energies for Li and Na atoms, preventing clustering. Results reveal that charge transfer from Li and Na to $BC_4N$ surface. $H_2$ adsorption on Li/$BC_4N$ and Na/$BC_4N$ systems shows non-dissociative behavior. The calculated hydrogen storage gravimetric density suggests significant storage capacities for both Li/$BC_4N$ and Na/$BC_4N$. Desorption temperatures are determined, providing insights for practical applications. Overall, co-doped graphene $BC_4N$ emerges as a promising material for efficient and practical hydrogen storage.

## Computational details

The study involves a comprehensive geometry optimization of various structures, conducted using the B3LYP/6–31 g(d, p) level of theory. The calculations are executed through the Gaussian 09 code[43]. The study also incorporates the dispersion correction method known as DFT-D3, based on the Grimme scheme[44]. This method is employed to accurately account for weak van der Waals interactions occurring between $H_2$ molecules and the substrates under consideration.

The focus of the investigation is on co-doped graphene, where non-bonded B and N atoms ($BC_4N$) are present, and these structures are terminated with hydrogen atoms. The binding energy ($E_b$) between lithium and sodium decorated BC4N monolayers calculated are shown as following:-

$$E_b = E_{M/BC4N} - (E_{BC4N} + E_M) \tag{3}$$

Where $E_{M/BC4N}$, $E_{BC4N}$, and $E_M$ are the total energies of Li, Na decorated $BC_4N$, energy of $BC_4N$, and energy of the isolated decorated-atom respectively.

The calculation of hydrogen adsorption energy ($E_{ads}$) on a Li, and Na over the stable position was calculated using equation:

$$E_{ads} = E_{H2\$M/BC4N} - (E_{M/BC4N} + E_{H2}) \tag{4}$$

Where $E_{H2\$M/BC4N}$, $E_{M/BC4N}$, and $E_{H2}$ are referred to the $H_2$ molecules adsorbed on decorated atom, and the energy of the free $H_2$ molecules respectively.

Charge density difference (CDD) plots were utilized to investigate the electron rearrangement accompanying $H_2$ adsorption. The CDD was computed as[38].

$$\Delta\rho = \rho_{3H2\$M/BC4N} - \rho_{M/BC4N} - \rho_{3H2} \tag{5}$$

Where $\rho_{3H2\$M/BC4N}$ is the total charge density of the Li, and Na decorated $BC_4N$ sheet with three adsorbed $H_2$ molecules, and $\rho_{M/BC4N}$ and $\rho_{3H2}$ are those of the Li, and Na decorated BC4N sheet and gas phase $H_2$ cluster, respectively.

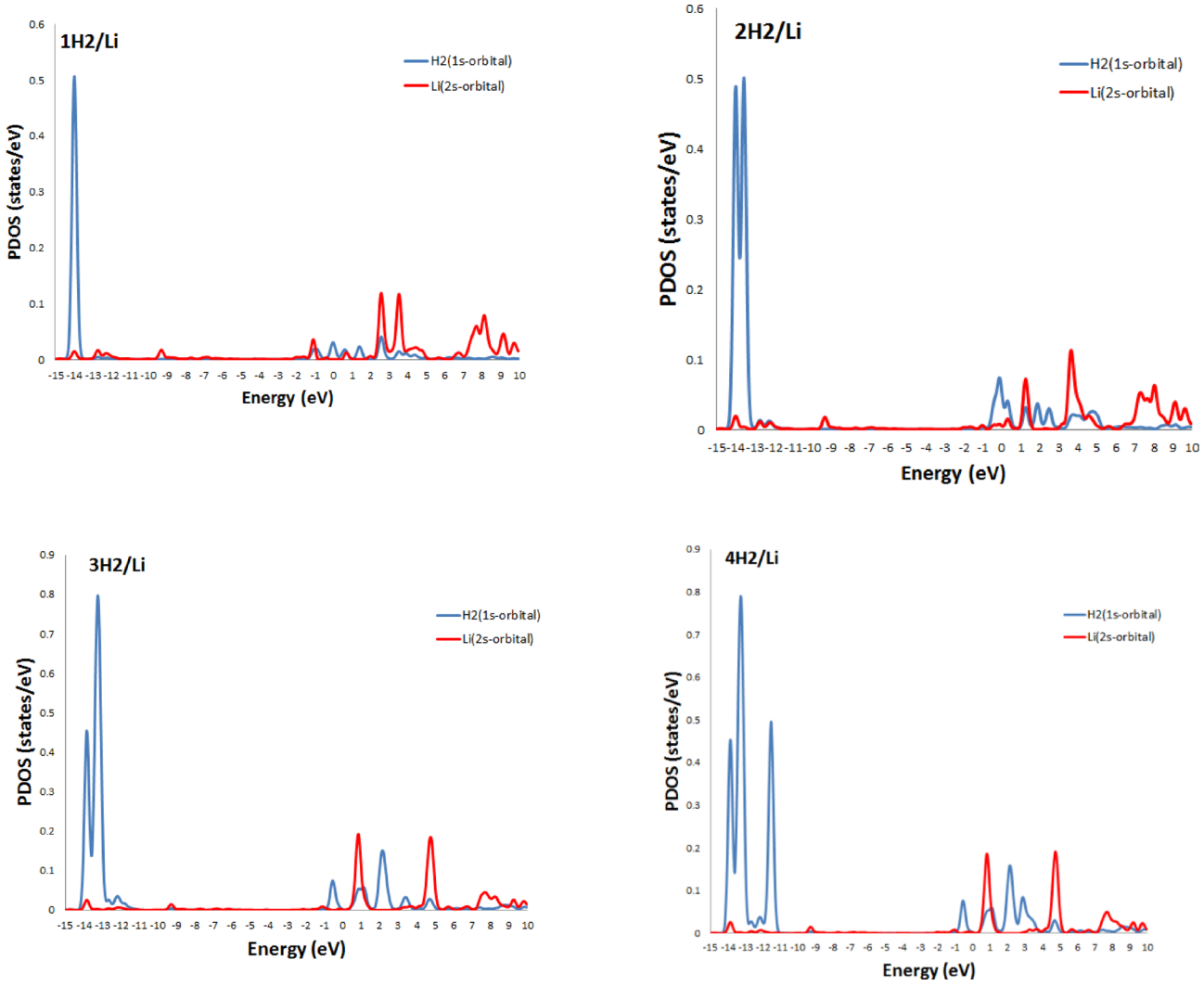


**Fig. 6**. PDOS of $H_2$ molecules on Li/$BC_4N$ monolayer.

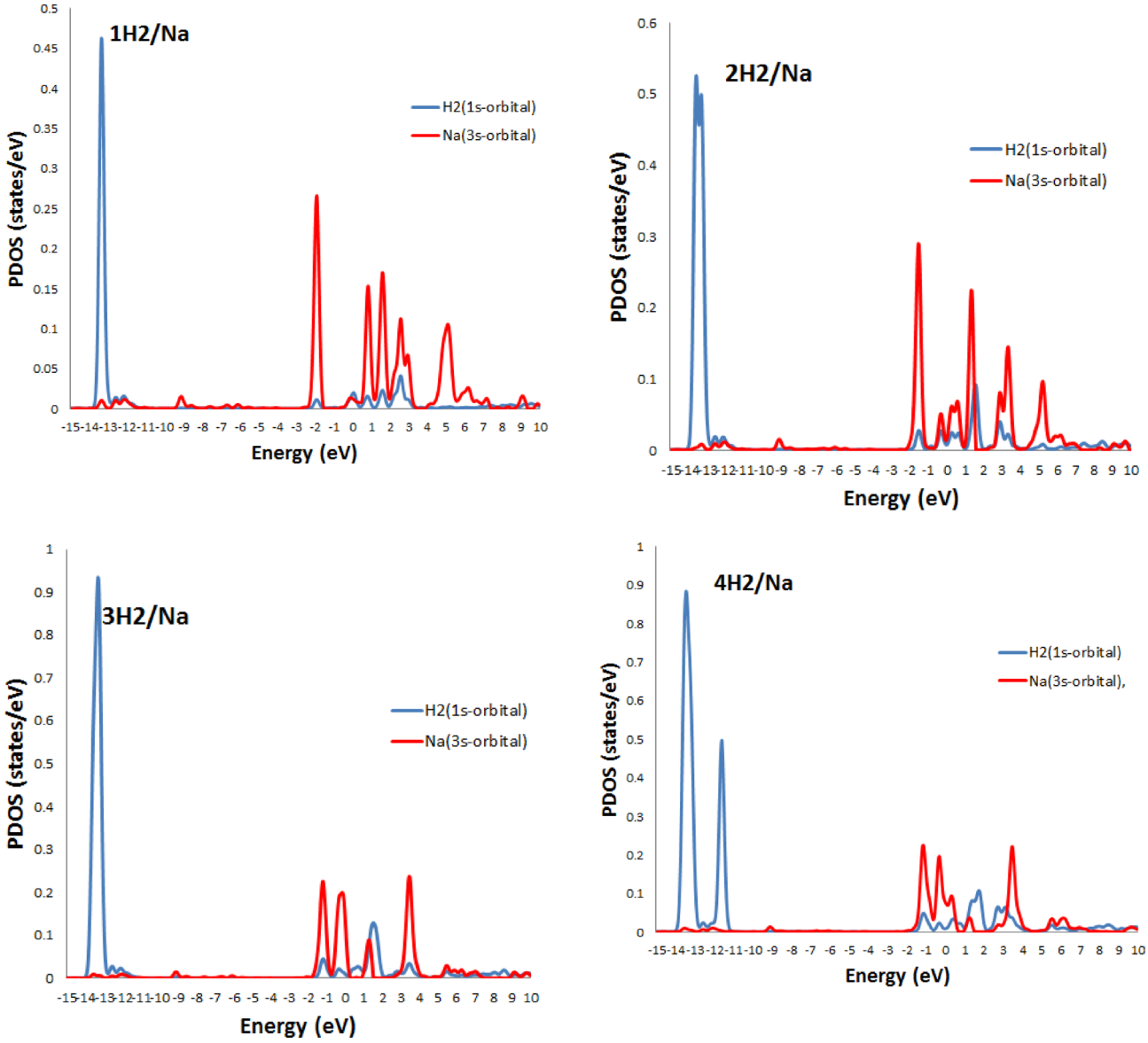


**Fig. 7**. PDOS of $H_2$ molecules on Na/$BC_4N$ monolayer.

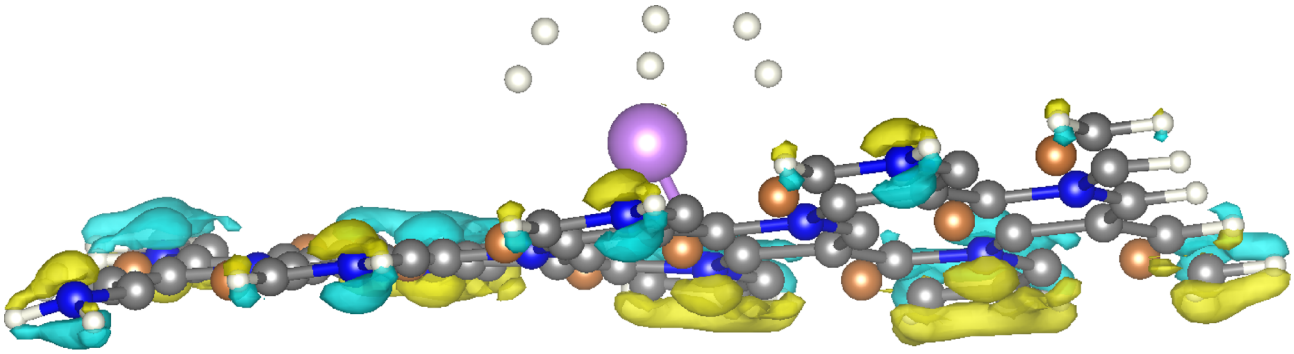

$3H_2$\$Li/$BC_4N$

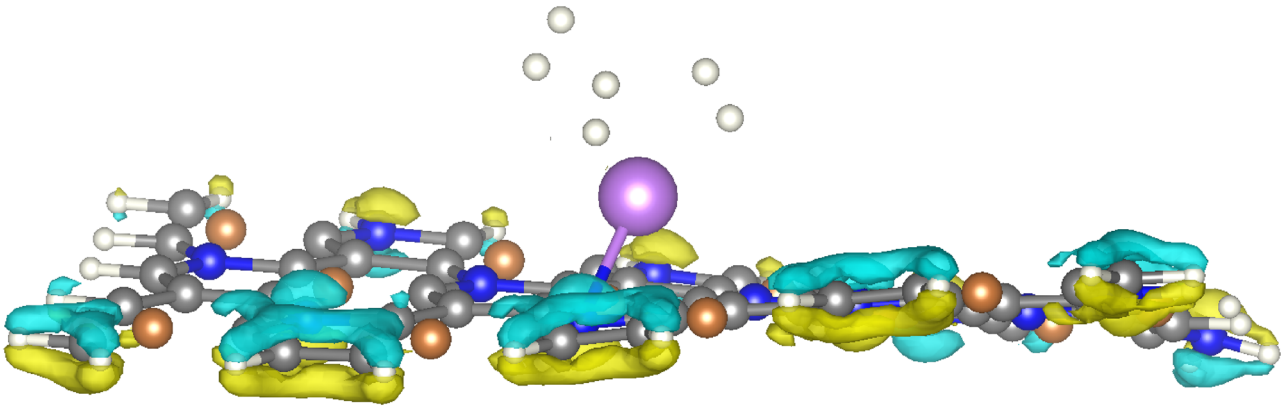

$3H_2$\$Na/$BC_4N$

**Fig. 8**. The Charge density difference of $3H_2$ on Li, and Na decorated $BC_4N$.

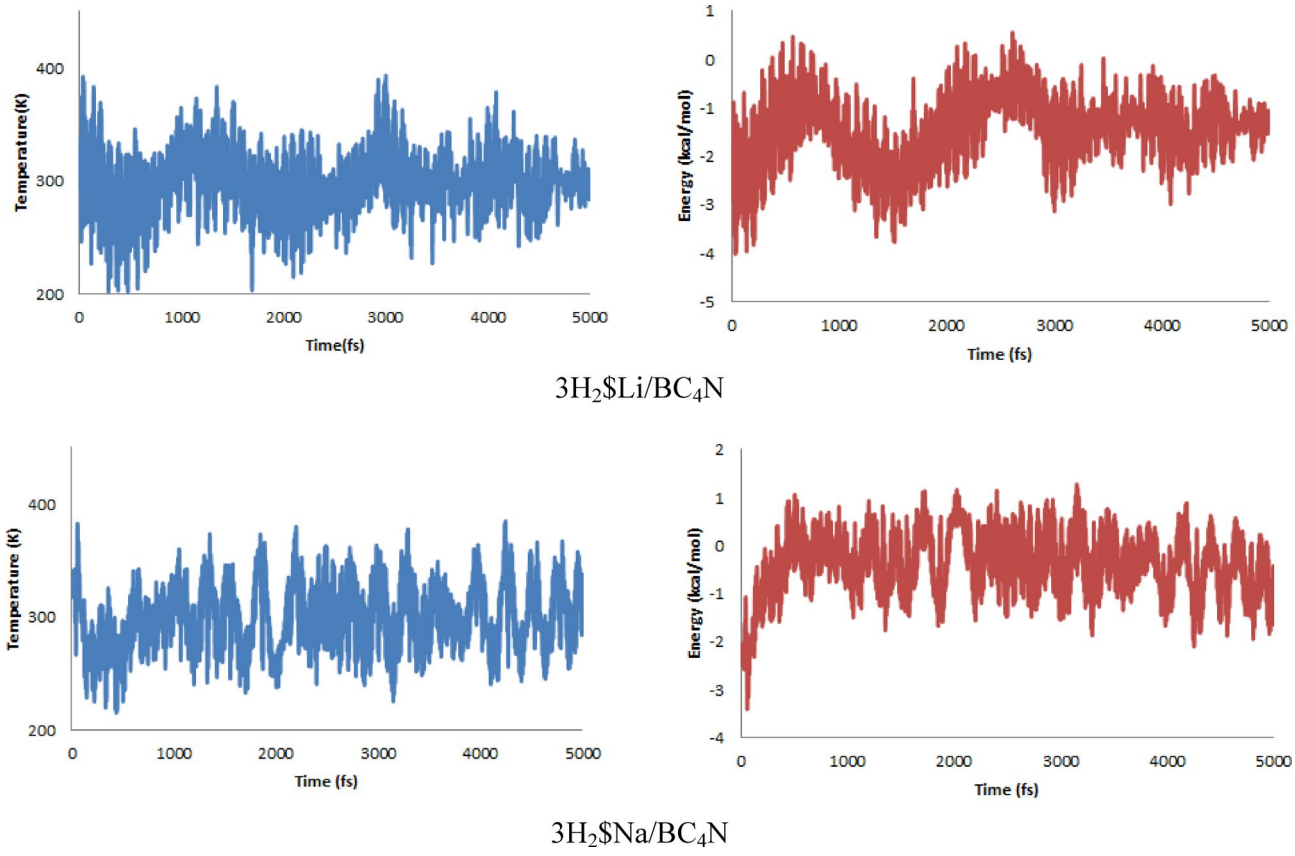


**Fig. 9**. Temperature and Energy profiles from AIMD simulations of 3H2 on Li, and Na decorated BC4N.

## Data availability

No datasets were generated or analysed during the current study.

Received: 13 April 2025; Accepted: 29 July 2025
Published online: 19 August 2025

## References

1. Zhou, Y. et al. Enhanced hydrogen storage on Li-doped defective graphene with B substitution: A DFT study. *Appl. Surf. Sci.* **410**, 166–176 (2017).
2. Zheng, N. et al. A DFT study of the enhanced hydrogen storage performance of the Li-decorated graphene nanoribbons. *Vacuum* **171**, 109011 (2020).
3. Choudhary, A. et al. First principles calculations of hydrogen storage on Cu and Pd-decorated graphene. *Int. J. Hydrog. Energy*. **41** (39), 17652–17656 (2016).
4. van den Berg, A. W. C. & Areán, C. O. *Materials for hydrogen storage: current research trends and perspectives*. *Chem. Commun.*, **6**, 668–681 (2008).
5. Jiang, M. et al. *Light metal decorated graphene-like Si2BN monolayers as hydrogen storage media: A DFT investigation*. *Int. J. Hydrog. Energy.*, **50**, 865-878 (2023).
6. Reshak, A. H. et al. First-principles calculations of structural, elastic, electronic, and optical properties of perovskite-type KMgH3 crystals: novel hydrogen storage material. *J. Phys. Chem. B.* **115** (12), 2836–2841 (2011).
7. Parkar, P. & Chaudhari, A. Reversible hydrogen storage on multiple Ti-doped B12C6N6 nanocage. *J. Energy Storage*. **62**, 106910 (2023).
8. Lee, H. et al. Ab initio study of dihydrogen binding in metal-decorated polyacetylene for hydrogen storage. *Phys. Rev. B*. **76** (19), 195110 (2007).
9. Fair, K. M. et al. Hydrogen adsorption capacity of Adatoms on double carbon vacancies of graphene: A trend study from first principles. *Phys. Rev. B*. **87** (1), 014102 (2013).
10. Xu, W. C. et al. Investigation of hydrogen storage capacity of various carbon materials. *Int. J. Hydrog. Energy*. **32** (13), 2504–2512 (2007).
11. Ozturk, Z. et al. Hydrogen storage in heat welded random CNT network structures. *Int. J. Hydrog. Energy*. **40** (1), 403–411 (2015).
12. Liang, H. et al. Manipulating active sites on carbon nanotube materials for highly efficient hydrogen storage. *Appl. Surf. Sci.* **619**, 156740 (2023).
13. Liu, M. et al. Novel 1D carbon nanotubes uniformly wrapped nanoscale MgH2 for efficient hydrogen storage cycling performances with extreme high gravimetric and volumetric capacities. *Nano Energy*. **61**, 540–549 (2019).
14. Tang, L. et al. A DFT study on defects and N doping to enhance hydrogen storage in Mg-decorated graphene. *Appl. Surf. Sci.* **648**, 159078 (2024).
15. Ao, Z. et al. Hydrogen storage in porous graphene with al decoration. *Int. J. Hydrog. Energy*. **39** (28), 16244–16251 (2014).

16. Zheng, Q., Wang, X. & Gao, S. Adsorption equilibrium of hydrogen on graphene sheets and activated carbon. *Cryogenics* **61**, 143–148 (2014).
17. Zheng, Q. et al. Analysis of adsorption equilibrium of hydrogen on graphene sheets. *Int. J. Hydrog. Energy*. **38** (25), 10896–10902 (2013).
18. Bonaccorso, F. et al. Production and processing of graphene and 2d crystals. *Mater. Today*. **15** (12), 564–589 (2012).
19. Chu, Y. et al. Mechanical properties of hydrogen Edge–Passivated chiral graphene nanoribbons. *J. Nanomechanics Micromechanics*. **5** (4), 04015001 (2015).
20. Ashna, G. E. et al. Hydrogen adsorption on vacancy-bent graphene nanosheets: A DFT study. *Mater. Today Commun.* **37**, 107319 (2023).
21. Chakraborty, B. et al. High capacity reversible hydrogen storage in titanium doped 2D carbon allotrope Ψ-graphene: density functional theory investigations. *Int. J. Hydrog. Energy*. **46** (5), 4154–4167 (2021).
22. Sterlin Leo Hudson, M. et al. Hydrogen uptake of reduced graphene oxide and graphene sheets decorated with Fe nanoclusters. *Int. J. Hydrog. Energy*. **39** (16), 8311–8320 (2014).
23. Ismail, N., Madian, M. & El-Shall, M. S. Reduced graphene oxide doped with ni/pd nanoparticles for hydrogen storage application. *J. Ind. Eng. Chem.* **30**, 328–335 (2015).
24. Parambhath, V. B. et al. Investigation of spillover mechanism in palladium decorated hydrogen exfoliated functionalized graphene. *J. Phys. Chem. C.* **115** (31), 15679–15685 (2011).
25. Jung, H. et al. Bio-inspired graphene foam decorated with Pt nanoparticles for hydrogen storage at room temperature. *Int. J. Hydrog. Energy*. **41** (9), 5019–5027 (2016).
26. Huo, Y. et al. Boron-doping effect on the enhanced hydrogen storage of titanium-decorated porous graphene: A first-principles study. *Int. J. Hydrog. Energy*. **46** (80), 40301–40311 (2021).
27. Du, A., Zhu, Z. & Smith, S. C. Multifunctional porous graphene for nanoelectronics and hydrogen storage: new properties revealed by first principle calculations. *J. Am. Chem. Soc.* **132** (9), 2876–2877 (2010).
28. Beheshti, E., Nojeh, A. & Servati, P. A first-principles study of calcium-decorated, boron-doped graphene for high capacity hydrogen storage. *Carbon* **49** (5), 1561–1567 (2011).
29. Wang, L., Yang, F. H. & Yang, R. T. Hydrogen storage properties of B- and N-doped microporous carbon. *AIChE J.* **55** (7), 1823–1833 (2009).
30. Wu, H. Y. et al. DFT study of hydrogen storage by spillover on graphene with Boron substitution. *J. Phys. Chem. C.* **115** (18), 9241–9249 (2011).
31. Lee, S. et al. Effect of nitrogen induced defects in Li dispersed graphene on hydrogen storage. *Int. J. Hydrog. Energy*. **38** (11), 4611–4617 (2013).
32. Shao, Y. et al. Progress in Nonmetal-Doped graphene electrocatalysts for the oxygen reduction reaction. *ChemSusChem* **12** (10), 2133–2146 (2019).
33. Zhao, Y. et al. Can Boron and nitrogen Co-doping improve oxygen reduction reaction activity of carbon nanotubes?? *J. Am. Chem. Soc.* **135** (4), 1201–1204 (2013).
34. Seenithurai, S. et al. Li-decorated double vacancy graphene for hydrogen storage application: A first principles study. *Int. J. Hydrog. Energy*. **39** (21), 11016–11026 (2014).
35. Wang, F. et al. Li-decorated porous graphene as a high-performance hydrogen storage material: A first-principles study. *Int. J. Hydrog. Energy*. **42** (15), 10099–10108 (2017).
36. Chan, K. T., Neaton, J. B. & Cohen, M. L. First-principles study of metal Adatom adsorption on graphene. *Phys. Rev. B*. **77** (23), 235430 (2008).
37. Zhang, H. et al. First-principles study of sodium adsorption and diffusion on vacancies, N, S, and NS-codoped graphene. *Mater. Today Commun.* **32**, 103817 (2022).
38. Dange, D., Beniwal, P. & Dhilip Kumar, T. J. Efficient hydrogen storage in superalkali NLi4-Decorated Boron phosphide biphenylene. *ACS Appl. Energy Mater.* **8** (11), 7594–7604 (2025).
39. Durgun, E., Ciraci, S. & Yildirim, T. Functionalization of carbon-based nanostructures with light transition-metal atoms for hydrogen storage. *Phys. Rev. B*. **77** (8), 085405 (2008).
40. Mahamiya, V. et al. Remarkable enhancement in catechol sensing by the decoration of selective transition metals in biphenylene sheet: A systematic first-principles study. *J. Phys. D*. **55** (50), 505401 (2022).
41. Naderizadeh, A., Baizaee, S. M. & Kahnouji, H. Density functional theory study of reversible hydrogen storage in monolayer beryllium hydride by decoration with Boron and lithium. *Int. J. Hydrog. Energy*. **48** (20), 7400–7418 (2023).
42. Faye, O. & Szpunar, J. A. An efficient way to suppress the competition between adsorption of H2 and desorption of nH2–Nb complex from graphene sheet: A promising approach to H2 storage. *J. Phys. Chem. C.* **122** (50), 28506–28517 (2018).
43. Frisch, M. J. et al. *Gaussian 09 Rev. D.01* (Wallingford, 2009).
44. Grimme, S. et al. A consistent and accurate Ab initio parametrization of density functional dispersion correction (DFT-D) for the 94 elements H-Pu. *J. Chem. Phys.* **132** (15), 154104 (2010).

## Author contributions

N. N. Mostafa: Methodology, Validation, Formal analysis, Investigation, Data Curation, Visualization, Writing - Original Draft; Kamal A. Soliman: Conceptualization, Methodology, Writing - Review & Editing; S.M. Abd El Haleem: Conceptualization, Supervision, Writing - Review & Editing; W.S. Abdel Halim: Conceptualization, Validation, Supervision, Writing - Review & Editing.

## Funding

Open access funding provided by The Science, Technology & Innovation Funding Authority (STDF) in cooperation with The Egyptian Knowledge Bank (EKB).

## Declarations

## Competing interests

The authors declare no competing interests.

## Additional information

**Supplementary Information** The online version contains supplementary material available at https://doi.org/10.1038/s41598-025-14088-8.

**Correspondence** and requests for materials should be addressed to K.A.S. or W.S.A.H.